Single-electron detachment cross sections for 5–50-keV H^- ions incident on helium, neon, and argon atoms

T. J. Kvale, J. S. Allen, X. D. Fang, A. Sen, and R. Matulioniene
Department of Physics and Astronomy, University of Toledo, Toledo, Ohio 43606
(Received 21 March 1994; revised manuscript received 12 August 1994)

Absolute measurements of the total single-electron detachment (SED) cross sections σ_{-10} for 3–50-keV H^- ions incident on helium atoms and for 5–50-keV H^- ions incident on neon and argon atoms are reported in this paper. The present SED cross sections for helium and neon targets are of similar magnitude but have a different energy dependence. By contrast, the SED cross sections for argon targets are significantly larger than either of the other two target species reported in this paper. Comparisons are made with the previous measurements and calculations in the literature.

PACS number(s): 34.70.+e

I. INTRODUCTION

Single-electron detachment (SED) is the dominant charge-changing process in intermediate energy collisions between hydrogen negative ions and noble-gas atoms due to the low binding energy of the H^- ion. Experimentally, these collision systems are readily amenable to laboratory study, so it is not surprising that numerous measurements have been reported (for example, see Refs. [1–11]) of SED collisions between 2–50-keV H^- ions and noble-gas atoms. However, discrepancies exist between the previous experimental results which are outside their quoted uncertainties. From a theoretical physics perspective, the H^-–noble-gas collision systems are among the classes of negative-ion–atom collision systems requiring minimal approximations in the theoretical models. Thus studies of detachment in these collision systems should be useful for improving our understanding of the physics of charge-changing interactions. Currently, *ab initio* theoretical calculations which adequately describe detachment for this collision system at these energies are still needed, even though the comparable experimental measurements have existed for over 30 years. Recent reviews addressing these collision systems include Tawara and Russek [12], McDaniel, Mitchell, and Rudd [13], and Risley [14].

In this paper, we report measurements of the total cross sections for single-electron detachment (SED) σ_{-10} for 3–50-keV H^- ions incident on helium atoms and for 5–50-keV H^- ions incident on neon and argon atoms. In a companion paper [15], we report measurements of the total cross sections for double-electron detachment (DED) σ_{-11} for the same energy range and for the same target species that were obtained in conjunction with the SED measurements. The motivations behind this work are to provide accurate experimentally determined cross sections, and to address the discrepancies in the literature for the experimental data for the SED process. The present experimental technique of simultaneously detecting all three scattered-beam components permits absolute SED cross sections to be determined without relying on other measurements or theoretical approximations, as well as containing self-consistency checks in the experimentally determined cross sections.

II. EXPERIMENTAL METHOD

A. Apparatus and data-acquisition technique

The SED cross-section measurements were made on the University of Toledo–Negative-Ion Accelerator shown schematically in Fig. 1. Negative ions were extracted from a duoplasmatron ion source in the accelerator terminal and focused by an einzel lens to form an ion beam. The ions then entered a velocity filter, which was operated as a mass analyzer to select only the H^--ion component of the ion beam. The H^- ions were accelerated to the collision energy by a 0–50-kV power supply connected to the accelerator terminal, and then were directed into a gas target cell located inside the scattering chamber vacuum housing. The H^- ion beam was initially collimated by the 2.0-mm-diameter acceleration column entrance aperture and further collimated by two, 0.5-mm-wide, crossed slits 0.5 m prior to the target cell.

The gas target cell was constructed from a modified, stainless-steel, four-way nominal 1.33 in., metal seal-type cross, and was the region where the collisions of interest occurred. The H^- ions entered the target cell through a 1.0-mm-diameter knife-edge aperture and exited the target cell through a 1.2-mm-diameter knife-edge aperture at the other side of the cell. The entrance and exit aperture separation distance ($l = 3.10$ cm) is assumed to be the effective scattering length. Research grade target gas was admitted into the target cell through a solenoid valve connected to one arm of the target cell by 1/4-in.-diameter stainless-steel tubing. The gas pressure inside the target cell was measured by a capacitance manometer connected to a different arm of the target cell through 1/4-in.-diameter stainless-steel tubing. The signal conditioner displayed the target gas pressure and provided a feedback voltage to the solenoid valve controller which maintained the target cell pressure at a preset value. The

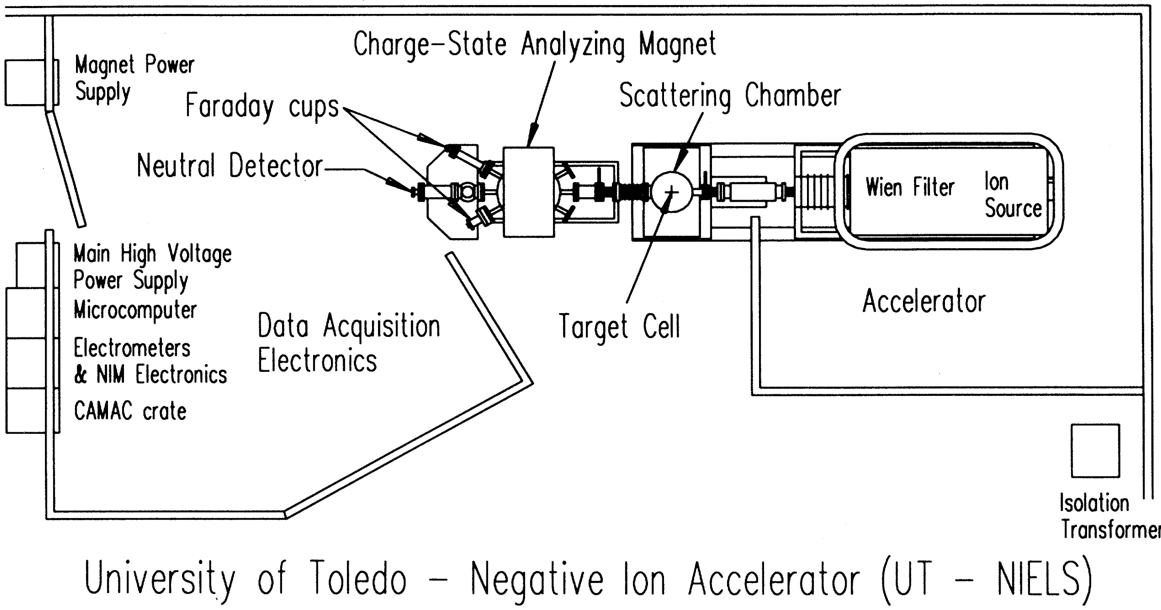

FIG. 1. Overview of the experimental apparatus.

target density n was obtained by means of the ideal gas law from the target gas pressure P and temperature T. The target thickness π is defined by $\pi=nl$, where n is the target gas density and l is the distance the beam has traversed in the gas (effective scattering length). The target thickness was varied over the range from $\pi=0$ to $\sim 3\times10^{14}$ atoms/cm^2 by changing the target gas pressure P in the target cell. For the target gas pressures used in the present experiment (typically ≤ 3 mTorr), the pressures inside the scattering chamber, as well as in the other beamline sections, were maintained at 10^{-6} Torr by five differential pumping systems.

After the incident beam exited the target cell, the fast, scattered beam entered the zero-degree, beam-entrance port of a dc laboratory magnet (charge-state analyzing magnet). The magnetic field of this magnet was adjusted to deflect the H^- and H^+ ion components into the $\pm 30°$ beam exit ports, whereas the H^0 atom beam passed undeflected through the magnet and entered the neutral detector connected to the 0°, beam-exit port of the magnet. This charge state separation of the scattered beam allowed all components of the scattered beam to be simultaneously detected by separate detectors for each of the three, charge-state component beams. The detection of all three scattered beams has the distinct advantage of allowing the SED total cross sections to be determined absolutely by two independent analysis methods without relying on other experiments and/or theoretical models.

Of the different methods available for the determination of the SED cross sections, the method used for the SED cross sections reported in this paper relied directly on the detection of the scattered H^0 atom beam ("direct method"). The conversion of the neutral H^0 atom current into an electrical signal was based on the principle of the secondary emission of electrons (and negative ions) which arose from the impact of an energetic H^0 atom beam on a metal surface. The neutral H^0 beam detector ("neutral detector") construction and operation were described in a separate paper [16]. The fast hydrogen atoms entered the neutral detector and struck a polished, copper cylinder target beveled at an angle of 30° with respect to the H^0 beam axis. The beveled surface was manually polished and had a "technical" surface grade. The inner shield of the neutral detector was biased at a positive voltage (10–50 V) relative to ground to attract the secondary negative particles away from the copper cylinder. This resulted in a net positive current to the copper cylinder (called the neutral detector current S_0 in this paper). The outer shield of the neutral detector was connected to ground.

The H^- ions exiting the charge-state analyzing magnet were deflected into a Faraday cup attached to one of the 30° exit ports. The protons resulting from double-detachment collisions were deflected into a similar Faraday cup attached to the other 30° exit port. The Faraday cup and neutral detector currents were measured by separate electrometers. The Faraday cup shields were biased at a negative voltage (≥ 50 V) relative to ground potential to suppress the secondary electrons and negative ions which were emitted when the fast ions struck the inner surfaces of the Faraday cups. Experimental tests were performed to verify that the measured H^- and H^+ ion currents represented the true H^- and H^+ beam currents to an uncertainty of less than 1%. During the course of this experiment, several different analog and digital electrometers were used to measure these currents, and no systematic effect in the cross-section values were attributed to the use of a specific electrometer.

For a fixed H^- ion impact energy, the beam-attenuation curve of the negative-ion current $I_{-1}(\pi)$ and the beam-growth curves of the proton current $I_1(\pi)$ and neutral detector current $S_0(\pi)$ were obtained by measuring these currents as a function of the target thickness. The incident H^- ion current $I_{-1}(0)$, the background H^+

ion current $I_1(0)$, and neutral detector current $S_0(0)$ were measured with no gas in the target cell before and after acquiring a set of growth and attenuation curves. The values of the background currents $I_1(0)$ and $S_0(0)$ were typically less than 0.1% and 3%, respectively, of the value of $I_{-1}(0)$. The value of $I_{-1}(0)$ typically changed by 1–5 % from the beginning to the end of a set of growth-curve measurements. The measured currents $I_{-1}(0)$, $I_1(0)$, and $S_0(0)$, the corresponding data for the growth $[S_0(\pi)$ and $I_1(\pi)]$ and attenuation $[I_{-1}(\pi)]$ curves, and the target pressure P were input into a microcomputer and together comprise what is referred to in this paper as a dataset. A typical dataset required about 15–20 min acquisition time. At each target cell pressure, the assumed instantaneous value of $I_{-1}(0)$ was obtained by linearly interpolating between the values of $I_{-1}(0)$ measured at the start and end of the dataset. After each dataset was acquired, the data were stored on disk for later entry into a separate analysis program (HDETACH3) for the determination of the resulting cross sections.

B. Scattered-beam fractions and analysis method

The charge-state composition of the incident ion beam evolves as it passes through the target gas due to charge-changing collisions with the target atoms. The scattered-beam fraction F_i is defined to be the background-subtracted flux of hydrogen ions or atoms with charge state i divided by the flux of incident H^- ions at zero target pressure:

$$F_i(\pi)\equiv\frac{[I_i(\pi)-I_i(0)]}{I_{-1}(0)}\ , \tag{1}$$

where i indicates charge states -1, 0, or 1. The neutral hydrogen atom ($i=0$) beam current is defined as $I_0\equiv S_0/\gamma$, where S_0 is the measured neutral detector current and γ is the secondary-negative-particle-emission yield ("yield") of the neutral detector. The electrical current I_0 is related to the H^0 atom current by dividing I_0 by the fundamental electric charge e. Assuming a pure incident H^- ion beam and at sufficiently low values of π, the solution to the scattered H^0 beam fraction rate equation is typically given as a quadratic function of target thickness (see for example, Ref. [13]):

$$F_0=\sigma_{-10}\pi+\tfrac{1}{2}[\sigma_{-11}\sigma_{10}-\sigma_{-10}(\sigma_{-10}+\sigma_{-11}+\sigma_{01}+\sigma_{0-1})]\pi^2\ , \tag{2}$$

where σ_{ij} is the total cross section for the charge-changing process $i\rightarrow j$. The F_0 growth curves are expected to have slightly negative curvatures with target thickness for all collision energies included in the present study due to the magnitudes of the various cross sections contributing to the quadratic coefficient. These curvatures are discussed in more detail in Ref. [17].

Because I_0 depends on the yield γ, the *apparent* SED cross section s_{-10} is obtained from the linear coefficient of a least-squares quadratic fit to the *apparent* neutral fraction γF_0 growth curve:

$$\frac{[S_0(\pi)-S_0(0)]}{I_{-1}(0)}=\gamma F_0=a_0+s_{-10}\pi+a_2\pi^2\ . \tag{3}$$

The absolute value for the *true* single-electron detachment cross section σ_{-10} is then determined from the *apparent* cross section s_{-10} and the yield γ by the relation $\sigma_{-10}=s_{-10}/\gamma$. The yield γ is not assumed to be known *a priori,* so s_{-10} was obtained for each dataset from the quadratic fit given in Eq. (3) and later converted to σ_{-10} after γ was determined. The present experimental technique has the advantage that the yield γ is obtained *in situ* from the growth-curve measurements by two independent analysis methods.

The method used to obtain γ (and consequentially for the determination of σ_{-10} from s_{-10}) relies on the fact that the total scattered current, comprised of the three charge-state beams, remains constant when the target thickness is changed slightly (typically about 0.2 mTorr). The yield is then determined from successive measurements of the currents $I_{-1}(\pi)$, $I_1(\pi)$, and $S_0(\pi)$ at slightly different target thicknesses π_1 and π_2, as given in the following equation:

$$\begin{aligned}\Delta N_T(\pi)&\equiv N_T(\pi_1)-N_T(\pi_2)\\&=0\\&=[I_{-1}(\pi_1)-I_{-1}(\pi_2)]+[S_0(\pi_1)-S_0(\pi_2)]/\gamma\\&\quad+[I_1(\pi_1)-I_1(\pi_2)]\ ,\end{aligned} \tag{4}$$

where the quantity $N_T(\pi)$ is the total scattered current at target thickness π. The measured secondary emission yield γ for a particular collision energy is obtained from a weighted average of all of the values of γ obtained from each dataset. Typically, over 100 individual measurements of γ were obtained at each collision energy. It is assumed that γ should be a smoothly varying function of incident H^0 energy, so the energy dependence of the secondary emission yield is obtained by a least-squares fit of the measured yields γ to a quadratic function of the logarithm of the H^0-atom energy (collision energy). The curves returned from this fit are

$$\gamma_{\mathrm{He}}=-0.4778+4.3186(\log_{10}E)-1.0286(\log_{10}E)^2 \tag{5}$$

for helium targets and

$$\gamma_{\mathrm{Ne,Ar}}=-0.1435+2.7424(\log_{10}E)-0.2548(\log_{10}E)^2 \tag{6}$$

for neon and argon targets, and E is the collision energy in keV. The quadratic fit in $\log_{10}E$ was chosen because it produced a satisfactory fit to the data over the present energy range. At each collision energy, no systematic variation in the secondary emission yield γ was observed over the time period of these measurements. The small difference between the yields γ for helium targets and for the neon and argon targets studied in this experiment is interesting. One possible explanation for the cause of the different yields γ is the difference in the relative populations of the metastable H(2s) state created in the collisions with the various noble-gas targets. Future studies are planned to investigate this hypothesis. The average deviation of the measured yields from the corresponding functional fits given in Eqs. (5) or (6) is 4.5%. The estimated uncertainty in the determination of the yield γ is taken to be this average deviation.

A second method of determining the yield γ is available in the present experimental technique and serves as an experimental check on γ obtained from the first method. The yield γ is determined from the total cross section ($\sigma_T=\sigma_{-10}+\sigma_{-11}$) obtained from the $F_{-1}(\pi)$ attenuation curve, the *apparent* cross section ($s_{-10}=\gamma\sigma_{-10}$) obtained from the growth curve of the *apparent* H^0-atom fraction, and the cross section (σ_{-11}) obtained from the $F_1(\pi)$ growth curve. Then

$$\gamma=\frac{s_{-10}}{[\sigma_T-\sigma_{-11}]} . \tag{7}$$

This method returned values of γ that are generally 2% higher than the values obtained from the first method given by Eqs. (5) and (6).

C. Error analysis

The uncertainties in the absolute values of the single detachment cross sections reported in this paper depend on the uncertainties in the measurements of the noble-gas target thickness and the hydrogen ion and atom currents. These uncertainties are summarized in Table I.

1. *Target thickness*

The noble-gas target thickness $\pi=nl$ is determined by the noble-gas pressure and temperature, and by the scattering length of the target cell. The manufacturer of the capacitance manometer used to measure the target gas pressure quotes [18] an absolute accuracy of ± 0.0132 mTorr for the present situation. The percent uncertainty in the pressure reading varies according to the actual pressure reading and a typical dataset was used to estimate an average uncertainty in the pressure reading. The uncertainty in the pressure reading for this dataset ranged from 0.5% at the maximum pressure to 4.6% at the lowest nonzero pressure. The average uncertainty is 1.4% and this uncertainty is taken to be the estimated overall uncertainty in the pressure reading. The capacitance manometer head is heated to 45 °C, and, in the present pressure range, a thermal transpiration correction of the pressure reading is necessary. The correction algorithm is given by Takaishi and Sensui [19] and Poulter *et al.* [20]. The correction typically amounted to about a 3% correction from the measured target cell pressure to obtain the true target cell pressure. The correction algorithm [19] was examined with the present data for neon targets at a collision energy of 25 keV. Precise (statistical uncertainties of order of 1%) single- and double-detachment cross-section measurements were obtained for H^- scattering from neon targets under the conditions of the capacitance manometer head at room (and target gas) temperature and at its operating (45 °C) temperature. The results of these measurements indicate that the data for which no correction factor was necessary and the corrected data are in fair agreement. The difference between the two sets of data (2%) is taken to be the uncertainty in the thermal transpiration correction of the neon target gas. Similar correction algorithms were applied to correct the target cell pressure readings for the helium and argon gas targets, but were not tested. The estimated uncertainty in the correction algorithm for the actual target cell pressure of the target gas is taken to be 2% for all three noble-gas target species. The temperature of the nobel gas in the target cell is assumed to be the same as the temperature of the target cell gas supply line, which is measured outside the scattering chamber housing. The uncertainty in the measurement of that temperature is 1%.

The uncertainty in the measured, geometric length of the target cell is $\leq 0.5\%$. Correction factors for the decrease in the effective scattering length l of cylindrical, gas-filled, scattering chambers with thin circular apertures due to the steady-state effusive flow of gas through the apertures have been calculated in Ref. [21]. Based on an extrapolation of the correction factors given in Ref. [21], the difference between the geometric and effective scattering lengths of the target cell used in the present experiments is estimated to be $\leq 0.5\%$. Because of the extrapolations and the lack of *in situ* measurements, the effective scattering length l is set equal to the geometric

TABLE I. Estimated systematic uncertainties in the experimental parameters comprising the total single electron detachment (SED) cross section σ_{-10}.

Parameter	Estimated systematic uncertainty (%)
Target thickness: (2.7%)	
Target pressure reading:	1.4
Target gas temperature:	1
Thermal transpiration correction:	2
Geometric scattering length:	0.5
Effective scattering length:	0.5
Ion and atom currents: (2.1%)	
Electrometer reading accuracy:	1.5
Secondary electron escape from the Faraday cups:	1
Angular scattering and misalignment of the Faraday cups:	1
Neutral detector secondary emission coefficient:	4.5
Total systematic uncertainty: (5.7%)	

length of the target cell in the present data, and the corresponding uncertainty is estimated to be 0.5%. The uncertainty in the measured values of π, obtained by adding the above uncertainties in quadrature, is 2.7%.

2. H^- and H^+ ion and H^0-atom currents

The uncertainties in the measurements of the ion and atom currents depend on the accuracy of the electrometers, the collection efficiency of the detectors, and the effect of beam losses due to misalignment of the beam or scattering of the hydrogen ions or atoms through angles greater than the solid angles of the detectors. The quoted accuracy of the calibrated electrometers used to measure the ion currents is 1.5%. From the measurements of the ion currents I_{-1} and I_1 as a function of the negative voltage applied to the shields of the Faraday cups, the secondary-electron collection efficiency of the Faraday cups was found to be greater than 99% when the negative shield bias voltage was greater than 50 V. This contributes an uncertainty of $\leq 1\%$ to the measurement of the H^- or H^+ ion currents.

If the H^- or H^+ ions are scattered through sufficiently large angles in the target cell, they will not be collected by the Faraday cups, and the measured ion currents will be lower than the actual ion currents. To check the effect of angular scattering on the ion current measurements, the H^+ and H^- ion currents collected by the Faraday cups were measured as a function of the magnetic field produced by the charge-state analyzing magnet. For the energy range of this experiment and a noble-gas target thickness of less than 5×10^{14} atoms/cm^2, no more than 1% of the H^+ and H^- ion currents should have been scattered outside the shield apertures (15.8 mm, i.d.) of the Faraday cups. The total ion uncertainty in the H^- and H^+ scattered-beam currents are obtained by adding the individual ion uncertainties in quadrature. These total ion uncertainties (2.1%) in the H^- and H^+ scattered-beam currents are assumed to be equal because of the present experimental arrangement.

The effects of misalignment and angular scattering on the measured H^0 atom rate I_0 were checked by comparing the current on the outer shield of the neutral atom detector with the neutral detector current S_0. For values of the noble-gas target thickness $\leq 3\times10^{14}$ atoms/cm^2, the current on the outer shield of the detector was found to be $\leq 0.01 S_0$ over the energy range of this experiment. Therefore the effects of misalignment and angular scattering contribute an uncertainty of about 1% to the measurement of the H^0 atom rate.

3. Total systematic uncertainty in the SED cross sections

The estimated total systematic uncertainty in the experimental values of σ_{-10} is assumed to be constant throughout the present energy range, and is obtained by adding in quadrature the uncertainties in π (2.7%), the ion and atom currents comprising the F_0 scattered H^0 beam fraction (2.1%), and the uncertainty in the secondary emission yield γ (4.5%). The total systematic uncertainty in the experimental values of σ_{-10} is then estimated to be 5.7%, assuming the independence of the component uncertainties listed above. This uncertainty is of the same order as the typical statistical uncertainty (2%) associated with the averaged measurements of σ_{-10}. It is noted that if the second method of determining γ is used, the resulting σ_{-10} cross sections will be systematically lower by about 2% from the quoted values given in Table II and shown in Fig. 2. The uncertainty in the collision energy is estimated to be 1%.

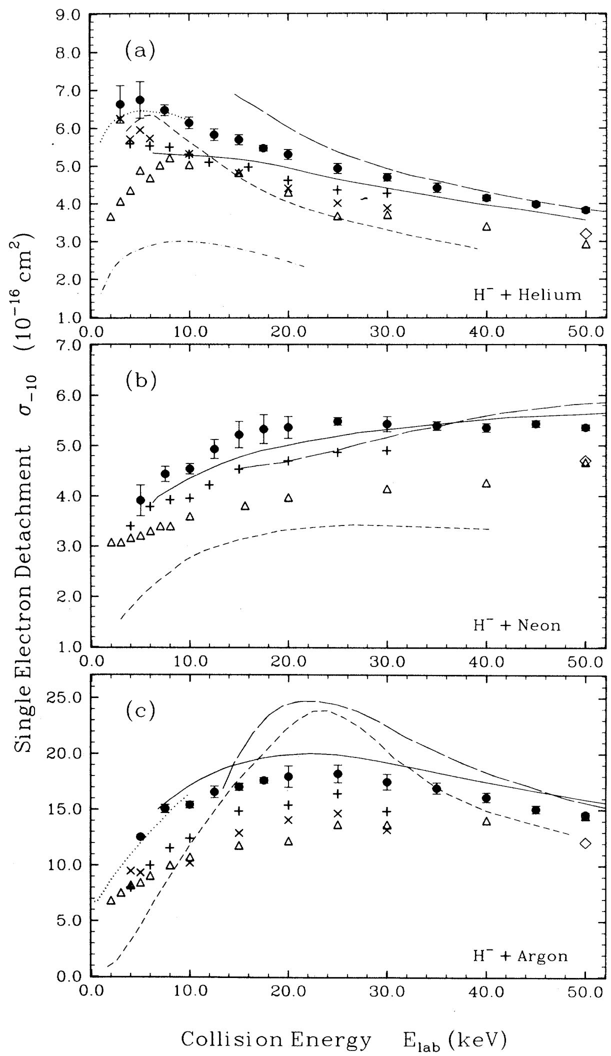

FIG. 2. Single-electron detachment cross sections σ_{-10} of H^- in collisions with (a) helium, (b) neon, and (c) argon target atoms, plotted as a function of the incident H^- ion kinetic energy. Experimental results: solid circles, present results; open triangles, Williams [1]; $\times$'s, Simpson and Gilbody [2]; dotted curve, Risley and Geballe [4]; diamonds, Anderson *et al.* [8]; pluses, Stier and Barnett [10]. Theoretical results: solid curves, Bates and Walker [26]; long dashes, Dewangan and Walters [27]; short dashes, Lopantseva and Firsov [23]; dot-dash, Sida [24].

TABLE II. Experimentally determined values of the total single-electron detachment (SED) cross sections σ_{-10} for H^- ions incident on helium, neon, and argon atoms. The uncertainties listed in the table are statistical uncertainties of one weighted standard deviation. The estimated systematic uncertainty in the cross-section measurements is 5.7%.

Collision energy $(\mathrm{keV})_{\mathrm{lab}}$	Target atom species Helium $(10^{-16}\ \mathrm{cm}^2)$	Neon $(10^{-16}\ \mathrm{cm}^2)$	Argon $(10^{-16}\ \mathrm{cm}^2)$
3.0	6.63±0.50		
5.0	6.75±0.48	3.91±0.31	12.53±0.14
7.5	6.47±0.14	4.43±0.15	15.07±0.37
10.0	6.14±0.15	4.54±0.11	15.41±0.29
12.5	5.83±0.15	4.93±0.19	16.57±0.53
15.0	5.70±0.13	5.22±0.26	17.02±0.32
17.5	5.47±0.08	5.33±0.29	17.60±0.29
20.0	5.30±0.13	5.37±0.22	17.96±0.95
25.0	4.93±0.13	5.49±0.07	18.21±0.79
30.0	4.69±0.10	5.43±0.15	17.48±0.70
35.0	4.41±0.12	5.40±0.09	16.93±0.50
40.0	4.15±0.07	5.36±0.09	16.11±0.42
45.0	3.98±0.06	5.43±0.07	15.08±0.34
50.0	3.83±0.06	5.36±0.05	14.58±0.19

III. RESULTS AND DISCUSSION

A. Present results

The present results for the absolute, total single-electron detachment (SED) cross sections, σ_{-10}, for 3–50-keV H^- ions incident on helium and 5–50-keV H^- ions incident on neon and argon atoms are plotted as a function of collision energy in Fig. 2 (solid circles) and are tabulated in Table II. The cross-section values are the weighted means from the F_0 growth curve quadratic fit analyses, and the corresponding statistical uncertainties are one weighted standard deviation [22]. The variance in the least-squares quadratic fit to each F_0 growth curve was used as the weighting factor for the cross section and their standard deviation determinations. A very small number of F_0 growth curves had the wrong curvature due to experimental difficulties, and were discarded prior to the averaging procedure. The estimated total systematic uncertainty in the present values of σ_{-10} is 5.7%, as discussed above.

A self-consistency check on the reported SED cross sections is possible because all three, exiting charge-state ($H^{-1,0,1}$), scattered beams were measured in the present experimental arrangement. An alternate experimental method of determining absolute SED cross sections is to measure the H^- attenuation curve to obtain the total detachment cross section, $\sigma_T(=\sigma_{-10}+\sigma_{-11})$, and independently measure the H^+ ion growth curve to obtain the double-detachment cross section σ_{-11}. The SED σ_{-10} is then obtained by numerical subtraction of σ_{-11} from σ_T. This method circumvents the experimental difficulty of measuring absolute H^0-atom currents, and is completely independent of the secondary emission yield γ. The SED cross sections obtained by this alternate method are in agreement with the direct method with average differences of -0.4% (helium—negative indicates that the direct method is lower than the alternate method), -3.4% (neon), and 7.2% (argon). It is noted that the averaged SED cross sections obtained by this alternate method display more fluctuations about a smooth energy dependence curve than those obtained by the direct (first) method. The agreement between the present results of the two, independent, experimental methods supports the quoted total systematic uncertainty (5.7%) in the present SED cross sections, as well as the absolute determination of the secondary emission yield γ.

In the analysis of the present data, the F_0 growth curves were fit to linear, quadratic, and cubic polynomials in target thickness to explore the functional dependencies of the growth curve. The linear-fit cross sections are lower than the quadratic-fit cross sections to the same growth curve data by average percent differences of 7.9% (helium), 7.6% (neon), and 18.8% (argon). The ratios of the averaged reduced chi squares χ_r^2 for the linear vs quadratic fits are 2.7 (helium), 4.5 (neon), and 45 (argon). Ratios greater than unity indicate that the averaged χ_r^2 for the quadratic fits are lower than the averaged χ_r^2 for the linear fits of the F_0 growth curves. This effect is expected due to the presence of a nonzero quadratic coefficient in the F_0 growth curves, as given in Eq. (2). By contrast, the ratios of the averaged χ_r^2 for the cubic vs quadratic fits are all close to unity, and the resulting cubic-fit cross sections are only slightly higher ($\leq 1.4\%$ for all three target gases) than the reported quadratic-fit cross sections. The differences between the cubic-fit cross sections and the present quadratic-fit cross sections are well within the systematic uncertainty of the measurements, and typically also within the statistical uncertainties. Thus for the present data, a quadratic functional fit satisfactorily accounts for the curvature in the F_0 growth curves.

B. Previous experimental results

Two experimental conditions greatly affect the determination or measurement of single-electron detachment (SED) total cross sections. The first is that all direct measurements of SED must relate the true, neutral H^0-atom current to the measured electrical signal. Direct measurements of the SED cross sections have been reported by Williams [1] and Simpson and Gilbody [2] in the 2–50-keV energy range and by Heinemeier, Hvelplund, and Simpson [7] and Anderson *et al.* [8] for impact energies of ≥ 50 keV. However, Williams [1] measured the relative values of σ_{-10} from 2–50-keV and then normalized the relative cross sections to the known absolute value of the electron capture cross section, σ_{10}, at 10 keV to obtain the absolute values of σ_{-10} shown in Fig. 2. Simpson and Gilbody [2] used the same particle detector for the measurement of both the H^0 scattered beam and the total scattered H^j ($j=-1,0,+1$) beam. The relative charge-state detection efficiency was checked by changing the target thickness and thereby changing the charge-state distribution of the total scattered beam.

An indirect method of experimentally determining the SED cross sections follows the alternate experimental method described in Sec. III A of this paper, which is to measure the H^- attenuation ($\sigma_T = \sigma_{-10} + \sigma_{-11}$) and the H^+ ion (σ_{-11}) growth curves. This method was employed by Lichtenberg, Bethge, and Schmidt-Böcking [9], who measured the total detachment cross section σ_T and the double-detachment cross section σ_{-11} by using two separate Faraday cups to detect the scattered H^- and H^+ ion beams after the two ion beams were electrostatically separated. The SED cross sections were then obtained by subtraction of σ_{-11} from σ_T. There is only one energy of overlap (50 keV), and the agreement between their results and the present results is excellent for helium targets.

Risley and Geballe [4] measured the H^- ion beam attenuation; however, all three scattered, charge-state, beam components were directed into one detector. Other experimental measurements were used in order to extract the SED σ_{-10} cross sections from their data. Stier and Barnett [10] also measured the attenuation of the H^- ion beam by electrostatic deflection of the surviving H^- ion beam in the gas target region. This removed the H^0 and H^+ charge-state components from the scattered beam. Other indirect, experimental methods rely on the detection of the detached electrons and slow, positive ions. An example of this experimental method is the work by Stedeford and Hasted [11].

The previous measurements can also be divided into two groups depending on the specific analysis of the scattered-beam growth curves that was used to obtain the reported SED cross sections. The F_0 growth curves have slightly negative curvatures, as explained by the magnitudes of the charge-changing cross sections comprising the quadratic coefficient given in Eq. (2). If a F_0 growth curve is fit to a linear function in the analysis, the deduced linear-fit total cross section will necessarily be lower than the cross section obtained from a quadratic fit. The cross sections reported by Williams [1], Simpson and Gilbody [2], and Anderson *et al.* [8], who derived the SED cross sections from a linear dependence on target thickness for the H^0-atom fraction, are lower than the present SED cross sections.

To further explore the consequences of the linear versus quadratic fits of the growth curves, a linear-fit analysis of the representative datasets were performed by reducing the upper limit of the target thickness range over which the F_0 growth curves were fit to obtain the single-electron detachment cross sections σ^L_{-10}. The σ^L_{-10} cross-section values obtained from one of the representative datasets are shown in Fig. 3 as solid circles located at the upper limit of the target thickness fit range. The line is a weighted fit to the deduced σ^L_{-10} cross-section values, where the number of target thicknesses in the range of the growth curve fit was used as the weighting factor. The arrows to the y axis indicate the values obtained from the linear fit of the entire target thickness range (4.658×10^{-16} cm^2) and the extrapolation of the linear-fit cross sections to zero target thickness

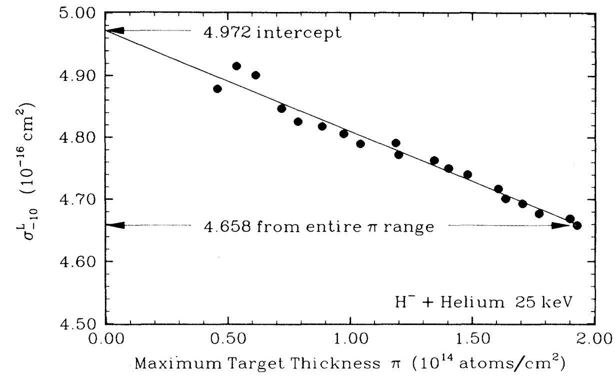

FIG. 3. The σ^L_{-10} cross sections obtained from linear fits to a typical F_0 growth curve for H^-+helium collisions as a function of reducing the maximum helium target thickness. Solid circles, total cross-section values from a linear fit of the growth curve data from zero target thickness up to the maximum target thickness used in the fit; solid line, weighted linear fit of the cross-section values obtained from the linear fits of the growth curve data.

(4.972×10^{-16} cm^2). The quadratic fit of the entire target thickness range gives a cross-section value of 4.965×10^{-16} cm^2, in excellent agreement with the extrapolated zero target thickness value of the linear-fit cross sections but well above the linear-fit cross sections for nonzero target thicknesses. This agreement is representative of all the datasets chosen for comparison, and this conclusion applies to all three target species. As seen in Fig. 3, the magnitude of the discrepancy for each individual growth-curve fit depends on the maximum target thickness used in the linear analysis fit. The χ^2_r test and the extrapolated linear-fit test both indicate that curvature is present even in the low target thickness region ("linear" region) of the scattered-beam growth curves and has a major effect (on the order of 10–20 %) on the reported cross-section values.

Other research groups have recognized the presence of curvature in the growth curves and stated that it must be accounted for in the analysis. Heinemeier, Hvelplund, and Simpson [7] allowed for the nonlinearity in the growth of the F_0 neutral fraction by hand fitting the neutral fraction divided by the target thickness [$F_0(\pi)/\pi$] to a linear function of the target thickness. The cross section σ_{-10} is then the F_0/π intercept. The experimental arrangement for their lower-energy measurements relied on a single position-sensitive detector to measure the scattered beams. There is only one energy of overlap (50 keV) between their results and the present results. The rather large discrepancy of 17% between these two cross-section values at 50 keV for helium targets is currently unexplained. Lichtenberg, Bethge, and Schmidt-Böcking [9] also accounted for curvature in the growth curves by fitting the data to nonlinear functions in target thickness. Stier and Barnett [10] quote the nonlinear rate equations for the attenuation of the incident H^- beam. However, if one interprets their Eq. (7) as their fitting function, then the H^- attenuation was only attributed to the SED process (i.e., $\sigma_T = \sigma_{-10}$) and all other charge-changing processes, including the double-detachment process, were neglected in their analysis. If this was their analysis method, then the quadratic coefficient in the expansion of the exponential would only involve $\frac{1}{2}\sigma_{-10}^2$, and the other cross-section pairs in the quadratic coefficient of the present Eq. (2) would be absent. The consequences of identifying $\sigma_T=\sigma_{-10}$ without accounting for all the charge-changing processes and fitting their growth curves to an exponential function would qualitatively explain why their results are generally higher than the linear-fit results and lower than the present results.

C. Theoretical calculations

The present, experimentally determined, single-electron detachment (SED) cross sections σ_{-10} are compared with various theoretical calculations for the SED cross sections σ_{-10} for collisions between H^- ions and helium, neon, and argon atoms in Figs. 2(a), 2(b), and 2(c), respectively. The calculations of Lopantseva and Firsov [23] predict much lower values for σ_{-10} in the cases of helium and neon targets, and the energy dependencies of the cross sections for helium and argon targets that are more pronounced than the present experimental results. The present values of σ_{-10} are a factor of 2 or more larger than the Born approximation calculations of Sida [24] and Bell, Kingston, and Madden [25], even though the calculations of Bell, Kingston, and Madden are only about 25% lower than the experimental data from other groups at collision energies above about 100 keV.

In the classical-impulse approximation calculations of Bates and Walker [26], the collision between the H^- ion and the target atom is modeled as an elastic collision between either electron of the H^- ion and the target atom. An assumption in this model is that the electrons in the H^- ion are equivalent, weakly bound electrons, and that the electrons are isotropically scattered. The results of this approximation, shown in Fig. 2 as the solid curves, are in fair agreement with the present values of the σ_{-10} cross sections for all three target species. Heinemeier, Hvelplund, and Simpson [7] presented an involved discussion of the Bates and Walker theory.

The semiempirical, free-collision model (FCM) calculations of Dewangan and Walters [27] are shown as the long dashed curves in Fig. 2. In contrast to the calculations of Bates and Walker, the FCM calculations of Dewangan and Walters include the contributions to the σ_{-10} cross sections due to both elastic and inelastic scattering of either electron of the H^- ion, and they do not assume that the electrons are scattered isotropically. Their σ_{-10} curves shown in Fig. 2 are calculated under the assumptions that one electron is weakly bound, with a binding energy of 0.755 eV, and that the other electron is strongly bound, with a binding energy equal to the binding energy of an electron in the ground state of the hydrogen atom.

IV. SUMMARY

The total cross sections for single-electron detachment (SED) in collisions between 3- and 50-keV H^- ions and helium atoms, and collisions of 5–50-keV H^- ions with neon and argon atoms are reported in this paper. The absolute SED cross sections have been measured by simultaneously measuring the growth of the H^0 atom and H^+ ion-scattered beam fractions and the attenuation of the H^- ion-scattered beam fraction as a function of target thickness. The measurements of all three curves are necessary to obtain absolute σ_{-10} cross sections and to have internal consistency checks on the reported cross sections. The growth curves for the H^0-atom fraction have a slightly nonlinear dependence on the target thickness which is well described by a quadratic function of the target thickness over the range of target thicknesses used in the present experiments. The SED cross sections for helium and neon targets are of the same order of magnitude, whereas the SED cross sections for argon targets are about a factor of 3–4 larger. The SED cross-section curves vary gradually with collision energy up to the maximum energy studied (50 keV). Of the calculations, the semiclassical calculation of Bates and Walker agrees best with the present cross sections in both magnitude and collision energy dependence. However, there still exists a need for *ab initio* calculations to adequately explain the mechanisms leading to the single-detachment process in these collision systems. With the determination of accurate SED total cross sections, *ab initio* calculations can now explore the extent to which the SED process is accompanied by excitation into the excited final states in the noble-gas target atoms, as well as SED into excited states of the resultant atomic hydrogen atoms, and thus gain a better understanding of the electron detachment process.

ACKNOWLEDGMENTS

The authors are appreciative of useful discussions with D. G. Seely, C. E. Theodosiou, and M. Kimura. This work is supported in part by the Division of Chemical Sciences, Office of Basic Energy Sciences, Office of Energy Research, U.S. Department of Energy.

[1] J. F. Williams, Phys. Rev. **154**, 9 (1967).
[2] F. R. Simpson and H. B Gilbody, J. Phys. B **5**, 1959 (1972).
[3] J. S. Risley, IEEE Trans. Nucl. Sci. **NS-26**, 1027 (1979).
[4] J. S. Risley and R. Geballe, Phys. Rev. A **9**, 2485 (1974).
[5] N. Andersen, T. Andersen, L. Jepsen, and J. Macek, J. Phys. B **17**, 2281 (1984).
[6] S. K. Allison, Rev. Mod. Phys. **30**, 1137 (1958).
[7] J. Heinemeier, P. Hvelplund, and F. R. Simpson, J. Phys. B **9**, 2669 (1976).
[8] C. J. Anderson, R. J. Girnius, A. M. Howald, and L. W. Anderson, Phys. Rev. A **22**, 822 (1980).

[9] W. J. Lichtenberg, K. Bethge, and H. Schmidt-Böcking, J. Phys. B **13**, 343 (1980).
[10] P. M. Stier and C. F. Barnett, Phys. Rev. **103**, 896 (1956).
[11] J. B. H. Stedeford and J. B. Hasted, Proc. R. Soc. London Ser. A **227**, 466 (1955).
[12] H. Tawara and A. Russek, Rev. Mod. Phys. **45**, 178 (1973).
[13] E. W. McDaniel, J. B. A. Mitchell, and M. E. Rudd, *Atomic Collisions—Heavy Particle Projectiles* (Wiley, New York, 1993).
[14] J. S. Risley, in *Electronic and Atomic Collisions*, edited by N. Oda and K. Takayanagi (North-Holland, Amsterdam, 1980), p. 619.
[15] J. S. Allen, X. D. Fang, A. Sen, R. Matulioniene, and T. J. Kvale (unpublished).
[16] J. S. Allen, X. D. Fang, and T. J. Kvale, Nucl. Instrum. Methods B **79**, 106 (1993).
[17] T. J. Kvale, J. S. Allen, A. Sen, X. D. Fang, and R. Matulioniene, the following paper, Phys. Rev. A **51**, 1360 (1994).
[18] *High Accuracy Pressure Measurement*, Bulletin No. 1360 1/89 (unpublished), available through MKS Instruments, Inc., Six Shattuck Road, Andover, MA 01810.
[19] T. Takaishi and Y. Sensui, Trans. Faraday, Soc. **59**, 2503 (1963).
[20] K. F. Poulter, M.-J. Rodgers, P. J. Nash, T. J. Thompson, and M. P. Perkin, Vacuum **33**, 311 (1983).
[21] B. P. Mathur, J. E. Field, and S. O. Colgate, Phys. Rev. A **11**, 830 (1975).
[22] P. R. Bevington, *Data Reduction and Error Analysis for the Physical Sciences* (McGraw-Hill, New York, 1969).
[23] G. B. Lopantseva and O. B. Firsov, Zh. Eksp. Teor. Fiz. **50**, 975 (1966) [Sov. Phys. JETP **23**, 648 (1966)].
[24] D. W. Sida, Proc. Phys. Soc. A **68**, 240 (1955).
[25] K. L. Bell, A. E. Kingston, and P. J. Madden, J. Phys. B **11**, 3357 (1978).
[26] D. R. Bates and J. C. Walker, Proc. Phys. Soc. **90**, 333 (1967).
[27] D. P. Dewangan and H. R. J. Walters, J. Phys. B **11**, 3983 (1978).